ARTICLE

Transparent, Flexible, and Highly Conductive Thin Films Based on Polymer−Nanotube Composites

Sukanta De,[†,‡] Philip E. Lyons,[†,‡] Sophie Sorel,[†] Evelyn M. Doherty,[†,‡] Paul J. King,[†] Werner J. Blau,[†,‡] Peter N. Nirmalraj,[‡,§] John J. Boland,[‡,§] Vittorio Scardaci,[∥] Jerome Joimel,[∥] and Jonathan N. Coleman[†,‡,*]

[†]School of Physics, [‡]CRANN, [§]School of Chemistry, Trinity College Dublin, Dublin 2, Ireland, and [∥]Hewlett-Packard DIMO, Liffey Park Technology Campus, Barnhall Road, Leixlip, Co Kildare, Ireland

ABSTRACT We have prepared flexible, transparent, and very conducting thin composite films from poly(3,4-ethylenedioxythiophene):poly(styrenesulfonate), filled with both arc discharge and HIPCO single-walled nanotubes, at high loading level. The films are of high optical uniformity. The arc discharge nanotube-filled composites were significantly more conductive, demonstrating DC conductivities of $>10^5$ S/m for mass fractions >50 wt %. The ratio of DC to optical conductivity was higher for composites with mass fractions of 55−60 wt % than for nanotube-only films. For an 80 nm thick composite, filled with 60 wt % arc discharge nanotubes, this conductivity ratio was maximized at $\sigma_{DC}/\sigma_{Op} = 15$. This translates into transmittance (550 nm) and sheet resistance of 75 and 80 Ω/□, respectively. These composites were electromechanically very stable, showing <1% resistance change over 130 bend cycles.

KEYWORDS: transparent film · flexible film · nanotube · conducting polymer · nanocomposite

Thin, transparent, conducting films play a huge role in modern electronics. Mainly used for electrode applications in devices such as liquid crystal displays, flat panel displays, plasma displays, touch panels, organic light-emitting diodes (OLEDs), and solar cells, they are also used as antistatic coatings and EMI shielding material. The most common material used in such applications is indium tin oxide (ITO). However, this material suffers from two considerable drawbacks. The first is economic: the price of indium has soared since 2001[1] and, despite a recent falloff, is expected to increase sharply in the future. The second is technical: in the future, display technology will move toward flexible, paper-like displays. ITO is completely unsuited for such applications due to its brittleness.[2,3]

Thus, it is clear that an ITO substitute is needed, preferably a material whose conductivity is invariant under flexing. To meet minimum industry standards, such a material should have a sheet resistance, $R_s \leq 100$ Ω/□, coupled with an optical transparency of $T \geq 90\%$ (550 nm). For thin conducting films, R_s and T are linked through[4,5]

$$T(\lambda) = \left(1 + \frac{188.5}{R_s}\frac{\sigma_{Op}(\lambda)}{\sigma_{DC}}\right)^{-2} \quad (1)$$

where σ_{Op} and σ_{DC} are the optical (generally quoted at 550 nm) and DC conductivities of the material, respectively. Using this equation, it becomes clear that these industry targets can only be met for a material with $\sigma_{DC}/\sigma_{Op} \geq 35$. The search for such a material has been ongoing for a number of years, with thin films of carbon nanotubes being the main candidate.[5−18]

Single-walled nanotube films typically have $\sigma_{Op} \sim 1.5 \times 10^4$ S/m.[10] Thus, to achieve $\sigma_{DC}/\sigma_{Op} \geq 35$ requires $\sigma_{DC} > 5.3 \times 10^5$ S/m, a significant challenge. However, while nanotube films have displayed σ_{DC}/σ_{Op} ratios of up to 10.1 for as-prepared films[10] and up to 25 for acid-treated films,[10] we are still some way off having a viable material. While acid-treated films have conductivity ratios approaching the target, these films may be unsuitable for OLED applications as the presence of residual mobile counterions can poison the emissive layer. In addition, nanotube films tend to be relatively porous[19] and have significant surface roughness,[10] properties that can be detrimental to certain electrode applications. In many ways, it would be preferable to have a polymer−nanotube composite film as the electrode. However, such composites have traditionally had low conductivities, typically <10 S/m,[20] and so low σ_{DC}/σ_{Op} ratios. Recently a number of papers have appeared which have broken this paradigm. This has happened in two ways. Blighe *et al.* demonstrated a filtration-based method to prepare very high volume frac-

*Address correspondence to colemaj@tcd.ie.

Received for review December 15, 2008 and accepted February 05, 2009.

Published online February 19, 2009. 10.1021/nn800858w CCC: $40.75

tion polymer−nanotube composite films.[21] Even while using an insulating matrix (polystyrene), these films demonstrated conductivities up to 10^4 S/m. The other method has been to use conducting polymers as matrices.[22] While composites prepared with small-ion-doped conducting polymers are unsuitable for use in applications such as OLEDs (see above), composites prepared from conducting polymers doped with large, immobile counterions pose no such problem. Such a polymer is poly(3,4-ethylenedioxythiophene) doped with poly(styrenesulfonate) (PEDOT:PSS). Here the PEDOT chains are positively charged, while the PSS chains are negatively charged. Recently,[23−26] PEDOT has been combined with carbon nanotubes to produce composites with conductivities of up to $\sim 7 \times 10^4$ S/m.[27] Such films displayed $\sigma_{DC}/\sigma_{Op} \sim 9$. While this result is impressive, we believe there is much room for improvement.

In this paper, we combine the two previous approaches to prepare high volume fraction composites from single-walled nanotubes (SWNTs) blended with PEDOT:PSS. We show that composites based on arc discharge SWNTs (Iljin nanotechnologies) are significantly more conductive than those based on HIPCO nanotubes (Unidym). These materials are the most conductive nanotube-based composites ever made ($\sigma_{DC} > 10^5$ S/m) and display $\sigma_{DC}/\sigma_{Op} \sim 15$. Finally, we show that these materials are elctromechanically stable, displaying no degradation of conductivity after prolonged flexing.

RESULTS AND DISCUSSION

Composite films were prepared by vacuum filtration from aqueous dispersions with PEDOT:PSS as the matrix and both Iljin and HIPCO SWNTs as the filler. For both filler types, films containing a range of mass fractions from 20 to 100% (nanotube only) were fabricated at a fixed nominal thickness, $t = 50$ nm. In addition, for a fixed mass fraction (55 wt % for HIPCO, 60 wt % for Iljin), films were prepared with a range of thicknesses. The PEDOT:PSS used in this work was purchased as a suspension of polymer nanoparticles, each a few tens of nanometers in diameter. It is important to verify that these polymer nanoparticles are not lost through the filter but remain to form part of the composite film. To check this, we prepared PEDOT:PSS films on cellulose membrane filters before transferring to polyethyleneterephthalate (PET) substrates. These films were electrically conductive, confirming the presence of PEDOT:PSS. In addition, Raman spectra ($\lambda_{ex} = 633$ nm) collected both on the filter and on PET showed the presence of PEDOT through its characteristic bands at 440 and 1420 cm^{-1} (see Figure 1A, top and middle). In addition, Raman spectra measured on Iljin/PEDOT:PSS composite films also showed the presence of these PEDOT:PSS bands. (NB these bands appear weak in the composite film due the relatively high intensity of the nanotube bands.) Thus, we believe the polymer to be retained on the filter to form composite films.

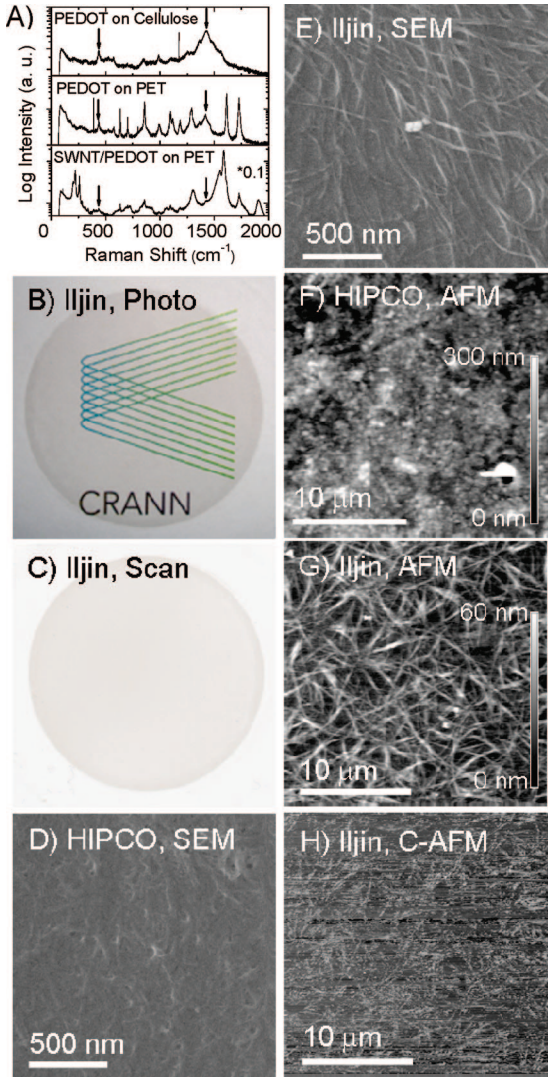

Figure 1. (A) Raman spectra of (top) a PEDOT:PSS film prepared by vacuum filtration on a cellulose filter, (middle) the same film after transfer to PET, and (bottom) an Iljin/PEDOT:PSS film prepared on a cellulose filter after transfer to PET. (B) Photo of a $t = 60$ nm, 60 wt % Iljin composite. (C) Transmission scan (150 dpi) of the same film as (B). SEM images of nominally 50 nm thick SWNT/PEDOT:PSS composite films prepared using (D) HIPCO nanotubes ($M_f = 55\%$) and (E) Iljin nanotubes ($M_f = 60\%$). AFM images of nominally 50 nm thick (F) HIPCO/PEDOT:PSS and (G) Iljin/PEDOT:PSS composite films. (H) Conductive AFM image of the same film area as (G).

A photograph of a typical composite film (60 wt % Iljin, $t = 60$ nm) is shown in Figure 1B. The high film quality is immediately apparent. To explore this in more detail, we made a transmission scan of the same film (Figure 1C). This scan is effectively a white light transmission map of the film with a resolution of 160 μm (150 dpi). The spatially averaged white-light transmittance was 81% for this film. The uniformity of the film is given by the standard deviation of the transmittance, calculated over the entire film area, which was 0.8%. The ratio of standard deviation transmission to mean

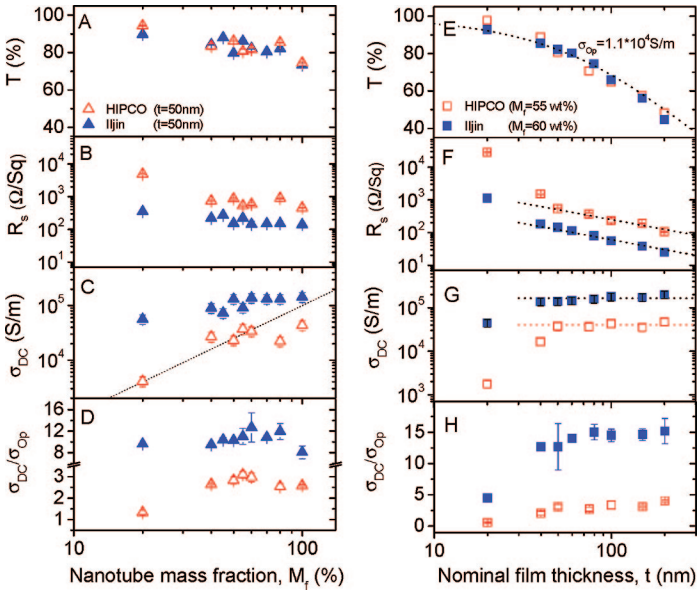

Figure 2. Optical and electrical data for PEDOT:PSS-based composites filled with both HIPCO and Iljin SWNT. (A) Transmittance (550 nm), (B) sheet resistance, and (C) DC conductivity as a function of nanotube mass fraction for films with nominal thickness of 50 nm. The dotted line in (C) illustrates quadratic behavior expected for percolating nanotube networks. (D) Ratio of DC to optical conductivity as calculated from the sheet resistance/transmittance data using eq 1 for both Iljin and HIPCO composites as a function of nanotube mass fraction. (E) Transmittance (550 nm), (F) sheet resistance, (G) DC conductivity, and (H) ratio of DC conductivity to optical conductivity as a function of film thickness for films of mass fraction 55% (HIPCO) and 60% (Iljin). The dotted line in (E) is a fit to eq 2. The dotted lines in (F) and (G) illustrate the behavior expected for bulk materials.

transmission was 1%. The low value of this quantity indicates the very high quality and optical uniformity of these composite films.

Shown in Figure 1D,E are representative SEM images of the surface of both HIPCO (M_f = 55%, t = 50 nm) and Iljin (M_f = 60%, t = 50 nm) based composites. For the HIPCO case, the network is hardly visible, appearing obscured by a polymer coating which fills much of the network free volume. For the Iljin composites, the polymer coating appears to be limited to a cylindrical shell surrounding the Iljin nanotubes. This disparity in coating may indicate differences between the surface energies of Iljin and HIPCO SWNTs or may simply be a reflection of differences in pore structure and/or size for the two film types. Nevertheless, both films have some free volume, making the surface of these films rough on the scale of tens of nanometers. Shown in Figure 1F is an AFM image of the surface of the HIPCO composite film shown in Figure 1D. The network is not resolved in this image due to the polymer coating. Note that considerable surface roughness can be seen in this image. For the Iljin composite, AFM images show a network of straight, well-defined bundles (Figure 1G). This network is considerably less rough than the HIPCO composite discussed above. Shown in Figure 1H is a conductive AFM current map of the area of the Iljin composite shown in Figure 1G. The current map of the Iljin film is very similar to the topographical map in Figure 1G, showing well-defined polymer-coated SWNT bundles which act as current paths out of the plane of the film. This is important as it shows that current can be gathered uniformly from all areas of the surface of these films—a critical property for any material with potential for use as an electrode. Surprisingly, it was impossible to detect a C-AFM signal from the HIPCO-based composites, perhaps due to the thick polymer coating.

These films were also characterized for both their electrical and optical transmission properties. For comparison, we initially characterized a 50 nm thick film of PEDOT:PSS. This displayed optical transmittance (λ = 550 nm) of 93% and sheet resistance of 3.7 M$\Omega/\square$, equivalent to a DC conductivity of 5 S/m. This is in line with what we expect for PEDOT:PSS without secondary doping.[28] For the composite films, optical transmittance *versus* wavelength spectra were flat and reasonably featureless for both composite types (similar to previously published spectra[24]). In general, as the nanotube mass fraction increased, the transmittance decreased while the spectral shape remained unchanged. The transmittance at λ = 550 nm is plotted as a function of mass fraction in Figure 2A for both composite types. In both cases, the data are similar, falling from 90−95% for the 10 wt % sample to ~75% for the 100 wt % sample. The sheet resistance, as measured on the same films, is shown in Figure 2B. In both cases, the sheet resistance falls slightly with increasing mass fraction. However, the Iljin composites are less resistive, falling to $R_s \sim 140\ \Omega/\square$ compared to a minimum value of ~450 $\Omega/\square$ for the HIPCO composites. We can calculate the nominal DC conductivity, σ_{DC}, from the sheet resistance using $\sigma_{DC} = 1/R_s t$, where t is the film thickness. This is shown in Figure 2C and emphasizes the higher conductivity associated with the Iljin composites, which reach a maximum value of 1.4×10^5 S/m compared to a maximum value of 4×10^4 S/m for the HIPCO composites. In both cases, the maximum in DC conductivity occurs for the nanotube-only film (100%). Interestingly, neither composite faithfully follows percolation-like scaling, the general form of which is shown by the dotted line.

In order to identify the optimum mass fraction for further studies, we use the data in Figure 2A,B to calculate σ_{DC}/σ_{Op} as a function of M_f, using eq 1. This is shown in Figure 2D for both composites. We note that σ_{DC}/σ_{Op} depends weakly on M_f, appearing to peak at 60 and 55 wt % for Iljin and HIPCO composites, respectively. We will discuss this in greater detail below.

With this in mind, we prepared films with mass fractions fixed at the optimized values (60 and 55 wt % for Iljin and HIPCO) for both composite types but with a range of nominal thicknesses from t = 20 to 200 nm. As before, for each film, the transmittance and sheet resistance were measured. Again, the transmittance spectra were relatively featureless. We plot the transmit-

tance at 550 nm as a function of nominal thickness in Figure 2E for both composites. Both data sets fall on the same curve, with T decreasing as t is increased. For thin conducting films, the transmittance is related to film thickness by[4,5]

$$T(\lambda) = (1 + 188.5\sigma_{Op}(\lambda)t)^{-2} \quad (2)$$

where σ_{Op} is the optical conductivity, a wavelength-dependent quantity which controls optical absorption. Equation 2 has been fitted to the data in Figure 2E as shown by the dotted line. Both data sets can be very well fit by eq 2, taking $\sigma_{Op} = (1.1 \pm 0.1) \times 10^4$ S/m ($\lambda = 550$ nm). This value is significantly lower than that of $\sigma_{Op} = 1.5 \times 10^4$ S/m ($\lambda = 550$ nm) found for neat films of SWNTs.[10,29] The sheet resistance data for the same films are shown in Figure 2F. In both cases, R_s falls with increasing t, with the Iljin composites significantly less resistive. Both data sets are well fit by $R_s = 1/\sigma_{DC}t$ for $t > 40$ nm, suggesting the film morphology becomes thickness invariant above this thickness. The nominal conductivity is shown in Figure 2G as a function of thickness. In line with the sheet resistance data, the conductivity is reasonably constant at higher values, falling off below $t = 40$ nm. These optimized films have mean conductivities ($t > 40$ nm) of $\sigma_{DC} = (1.65 \pm 0.2) \times 10^5$ and $(4.0 \pm 0.4) \times 10^4$ S/m for Iljin and HIPCO composites, respectively.

It is worth noting that these conductivities are extremely high even for composites with conducting matrices. Bulk composites prepared from SWNTs embedded in polyacrylonitrile have reached conductivities of 1.5×10^4 S/m.[22] Composites based on SWNTs embedded in PEDOT have also shown very high conductivities, reaching values of $\sim 7 \times 10^4$ S/m. However, to the authors' knowledge, this work is the first to demonstrate composite conductivities greater than 10^5 S/m. There are two main reasons why we achieve such high conductivities. The first is that we use Iljin nanotubes, which are well-known for their ability to form highly conductive nanotube films.[9] In fact, the state-of-the-art for nanotube films is for films prepared using Iljin SWNT, displaying conductivities as high as 2×10^5 S/m.[9] The second reason is that, building on our previous work,[21] we can attain nanotube mass fractions far in excess of any others reported in the literature. It is this combination of highly conductive tubes at high mass fraction that gives us such superlative properties.

We calculate σ_{DC}/σ_{Op} as a function of film thickness from the data in Figure 2E,F using eq 1. These data are shown in Figure 2H and scale with thickness in a fashion similar to the DC conductivity. At thicknesses above 80 nm, σ_{DC}/σ_{Op} saturates close to values of 15 and 3.3 for the Iljin and HIPCO composites, respectively.

As described above, many applications require low sheet resistance coupled with high transparency. To this end, we plot transmittance *versus* sheet resistance

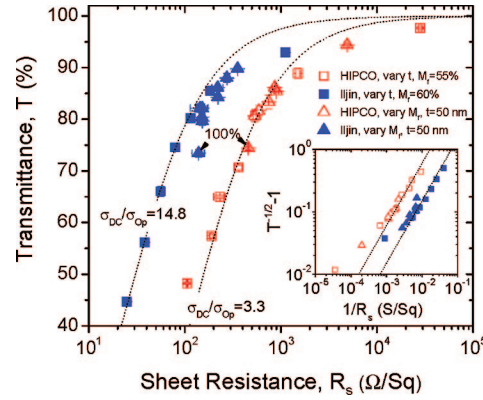

Figure 3. Transmittance (550 nm) plotted as a function of sheet resistance for all the samples measured in this work. The dotted lines are fits to eq 1. Inset: Transmittance *versus* sheet resistance data plotted to emphasize how well these data are fitted by eq 1. The dotted lines are equivalent to the fit lines in the main figure.

data for all four data sets (fixed t, varying M_f, and fixed M_f, varying t, for both nanotube types) in Figure 3. For each tube type, both data sets (varying both t and M_f) fall close to the same curve as illustrated by the dotted lines. The Iljin data, however, are shifted to lower R_s, in line with their higher conductivities. These data have been fitted using eq 1; the dotted lines in Figure 3 are consistent with $\sigma_{DC}/\sigma_{Op} = 14.8$ and 3.3 for the Iljin and HIPCO composites, respectively. These values are as expected from Figure 2H. It is interesting that the data found by varying M_f for fixed t also fall on this line. This can be seen more clearly by plotting the data as $T^{-1/2} - 1$ *versus* $1/R_s$ as shown in the inset of Figure 3. Here, data described by eq 1 should fall on a straight line. This is observed for all data (except for those films with the lowest values of t or M_f) with linearity illustrated by the dotted lines. This shows that, not only are the films prepared by varying t described by eq 2, but the films prepared by varying M_f are also. This is interesting as it shows that composites with different mass fractions of nanotubes tend to have similar values of σ_{DC}/σ_{Op}. Referring back to Figure 2D, we note that while σ_{DC}/σ_{Op} displays a clear peak for each composite its overall dependence on M_f is very weak. Thus, σ_{DC}/σ_{Op} only varies between 8 and 15 for the Iljin networks and between 1 and 3 for the HIPCO networks over the entire range of mass fraction. This relative invariance suggests that reductions in the mass fraction, while resulting in a more open nanotube network, do not significantly change the network topology or connectivity.

Another interesting point is that the data for the nanotube-only films fall close to, but slightly below (in a quality sense), these trend lines. This is in contrast to the vast majority of polymer−nanotube composites where the electrical properties are significantly reduced by the presence of polymer layers, which act as tunnelling barriers, between adjacent nanotubes.[20,30] That the electrical/optical properties of these composites are certainly not inferior but actually superior to the

nanotube-only films suggests that internanotube polymer layers do not significantly inhibit intertube electron transfer at nanotube junctions. We propose that this lack of tunnelling barriers, coupled with the reasonably low optical conductivity observed in composites, contributes to these high values of σ_{DC}/σ_{Op}. That σ_{DC}/σ_{Op} displays a peak when plotted *versus* mass fraction shows that the DC and optical conductivities scale differently with nanotube mass fraction. Thus, the balance between charge transport and light absorption is optimized at certain mass fractions ($\sigma_{DC}/\sigma_{Op} = 12.7$, $M_f = 60$ wt %, $t = 60$ nm). We note that this is higher than the value measured for Iljin-only films of the same thickness ($\sigma_{DC}/\sigma_{Op} = 8.1$, $M_f = 100$ wt %, $t = 60$ nm).

Overall, our highest value was $\sigma_{DC}/\sigma_{Op} = 15.0 \pm 1.2$ (Iljin, $M_f = 60$ wt %, $t = 80$ nm). This is significantly higher than both the highest published value of ~9 for simple polymer−nanotube composites[27] and the value of ~12 obtained for composites of lithium-doped SWNTs.[23] (In the previous two papers, σ_{DC}/σ_{Op} was not quoted. We calculated it from published R_s, T data.) We note that our value of $\sigma_{DC}/\sigma_{Op} = 15.0 \pm 1.2$ is higher even than the highest value reported for undoped SWNT-only films ($\sigma_{DC}/\sigma_{Op} = 10.1$).[10] To our knowledge, only data for acid-treated SWNT networks have resulted in higher values ($\sigma_{DC}/\sigma_{Op} = 25$).[10]

Finally, we note that while these composites are close to being a viable replacement for ITO they are potentially even more useful as a *flexible*, transparent, electrode material. Such a material is of considerable interest as an electrode in applications such as e-paper. To test this, we prepared composite films on PET using both Iljin and HIPCO nanotubes as filler ($t = 50$ nm, $M_{f,Iljin} = 60$ wt %, $M_{f,HIPCO} = 55$ wt %). In each case, we monitored the sheet resistance during bending with the composite film both in tension and in compression. The films were bent from an initial radius of curvature of 7.5 mm to a final radius of 2.5 mm before being relaxed. Shown in Figure 4A is the sheet resistance *versus* radius of curvature during both the bending and release phases (note that the magnitude of the average strain[31] felt by the film is plotted in the top axis). From these data, it is clear that the sheet resistance of the Iljin-based composites varies by <1% during both bend and release phases for films both in tension and in compression. In comparison, while the HIPCO films are very stable in tension, they undergo a reproducible reduction in resistance of ~10% while bending in compression. For comparison purposes, shown in the inset are data taken for an ITO film sputtered onto PET that was subjected to the same test. It is clear that the ITO fails catastrophically on tensile bending, with the sheet resistance increasing irreversibly by almost 2 orders of magnitude.

While these composite films are clearly relatively stable during one bend cycle, it is important to ascertain their stability over many bend cycles. Shown in Figure 4B is the mean sheet resistance per cycle plotted *versus* cycle number for the same films examined in Figure 4A. It is clear that the sheet resistance of the Iljin-based films varied by <1% over ~130 cycles. Similarly, the HIPCO-based composite subjected to tensile bending was also extremely stable. However, as before, the compressively bent HIPCO-based composite films were relatively unstable, undergoing increases in resistance of ~30% over 200 cycles. Note that none of these composites failed during these measurements. The number of cycles was limited by time constraints. For comparison, we show cyclic test data for an ITO/PET film in the inset. In this case, to avoid immediate failure, the film was tested at low curvature, with minimum bend radius of 20 mm on each cycle. In stark contrast to the composite films, the sheet resistance of this film increased by a factor of 8 before failing around cycle 150. These results can be compared to previously published results for (lower conductivity) PEDOT:PSS/SWNT films whose resistance increased by ~8% after 1800 bending cycles.[27]

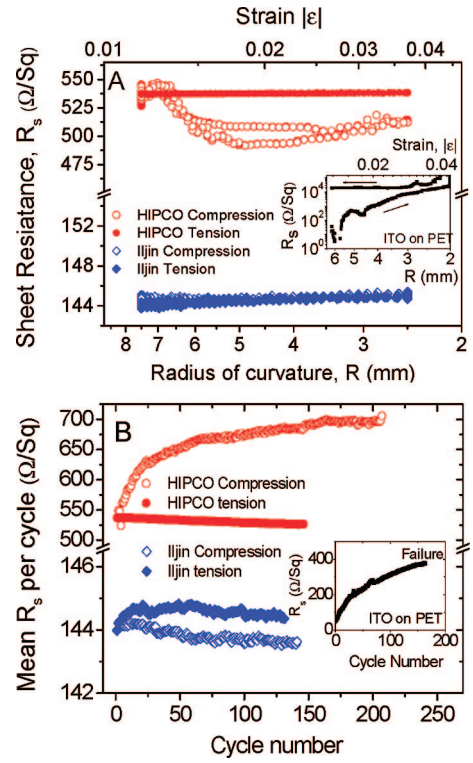

Figure 4. Electromechanical measurements made on composites with $t = 50$ nm and $M_f = 55\%$ (HIPCO) and $M_f = 60\%$ (Iljin). (A) Sheet resistance *versus* radius of curvature for one bend/release cycle measured for films both in compression and in tension. Inset: Results for a film of ITO on PET. (B) Mean sheet resistance per cycle as a function of cycle number for films in both tension and compression. Inset: Results for a film of ITO on PET.

CONCLUSION

We have demonstrated the preparation of thin composite films based on PEDOT:PSS doped with two different types of SWNTs. The spatial uniformity of the opti-

cal transmittance of these films is exceptional. We have measured the optical transmittance and sheet resistance as a function of both mass fraction and film thickness. While the optical properties of both composite types are similar, composites based on arc discharge tubes are significantly more conductive than those based on HIPCO tubes, reaching conductivities of 1.65×10^5 S/m. In both cases, we find the ratio of DC to optical conductivity is maximized for mass fractions of 55−60 wt %. The highest value found was $\sigma_{DC}/\sigma_{Op} = 15$, which was observed for an 80 nm thick film containing 60 wt % Iljin (arc) SWNTs. This film has transmittance and sheet resistance values of $T = 75\%$ and $R_s = 80\ \Omega/\square$. Electromechanical testing showed both composites to be extremely stable under flexing and cycling. In particular, the Iljin-based composites displayed sheet resistances which varied by less than 1% over 130 bend/release cycles. We believe that with moderate improvement such composites could be suitable for use as flexible electrodes in applications such as solar cells or displays.

METHODS

HIPCO SWNTs were purchased from Unidym (www.unidym-.com/), while Iljin SWNTs were purchased from Iljin Nanotech Co., Ltd. (http://www.iljinnanotech.co.kr/). PEDOT:PSS was purchased from HC Stark under the tradename Baytron PH500 (www.hcstarck.com). A stock solution of sodium dodecyl sulfate (SDS, Aldrich Batch #014k01141) of concentration 5 mg/mL in Millipore water was prepared by overnight stirring. Some of this solution was used to prepare a stock nanotube dispersion by adding SWNTs such that the SDS/SWNT mass ratio was 5:1 (starting nanotube concentration, $C_i = 1$ mg/mL). This dispersion was subjected to 5 min of high-power tip sonication (VibraCell CVX; 750 W, 20% 60 kHz). The dispersion was then placed in a sonic bath (Model Ney Ultrasonic) for 1 h and was then subjected to another 5 min of high-power sonication, before being allowed to rest overnight, followed by centrifugation at 5500 rpm for 90 min. The supernatant was carefully decanted and saved. The postcentrifuge nanotube concentration was determined from absorbance measurements (Cary 6000i).

Nanotube−PEDOT:PSS composite dispersions were subsequently prepared by mixing the required volume of nanotube stock solution and PEDOT:PSS dispersion, keeping the partial nanotube concentration in the composite dispersion at 0.005 mg/mL. Note that no secondary dopant was added to the PEDOT:PSS. This composite dispersion was then subjected to 1 min high-power sonication.

The composite films were prepared by vacuum filtration using porous cellulose filter membranes (MF-Millipore membrane, mixed cellulose esters, hydrophilic, 0.025 μm, 47 mm). The film thickness was controlled by the volume of dispersion filtered and hence the deposited nanotube mass. The deposited films were washed with 200 mL of Millipore water followed by a wet transfer[16] to a polyethyleneterephthalate (PET) substrate using heat and pressure. The cellulose filter membrane was then removed by treatment with acetone vapor and subsequent acetone liquid baths followed by a methanol bath. The final film diameter was 36 mm. The film thickness, t, was calculated from the deposited mass per unit area, M/A, using $M/A = \rho t$, where ρ is the film density. We estimate the film densities as 600−900 kg/m^3 for mass fractions from 0.8 to 0.2. These values are estimated by calculating the weighted average values of the densities of porous nanotube films (~450 kg/m^3)[19] and PEDOT:PSS (~1000 kg/m^3). We estimate the thickness to be correct to within 10%. This means that the DC and optical conductivities carry an error of 10%.

Transmission scans were made using an Epson Perfection V700 photo flat-bed transmission scanner. Scanning electron microscopy measurements were made using a Hitachi S-4300 field emission scanning electron microscope. Atomic force microscope images were obtained using a Veeco Nanoman AFM system. In order to extract the topography and conductance data simultaneously, the microscope was operated in the conductance imaging mode (C-AFM). In this technique, the AFM tip acts like a mobile probe on the surface and is held at ground potential, and a DC bias is applied to the sample. The z feedback signal is used to generate a normal contact mode AFM topographic profile, and the current passing between the tip and the sample is measured using a preamplifier to generate the conductance image. A bias voltage of 0.2 mV up to 1 V is applied to the electrode on the surface that drives current through the tubes. A current range of 2 pA to 1 μA can be detected by the preamplifier in the CI-AFM module. For this purpose, a Cr/Pt-coated conductive tip with a force constant of 3 N/m and a resonant frequency of 75 kHz was employed. In all cases, the loading force employed during measurement was approximately 15 nN. (The tips were purchased from Budget Sensors, ElectriMulti 75.) Optical transmission spectra were recorded using a Varian Cary 6000i. In all cases, a sheet of PET was used as the reference. Sheet resistance measurements were made using the four-probe technique with silver electrodes of dimensions and spacings typically of ~millimeters in size and a Keithley 2400 source meter. Electromechanical measurements were made using a Zwick Z0.5 Proline tensile tester. The composite film on PET was bent into a semicircle, which was constrained by the grips of the tensile tester. The film was connected *via* two electrodes (attached to the grips) to a Keithley KE 2601. The bend radius was then defined by the distance between the grips. The intergrip distance was then oscillated between typically 15 and 5 mm over many cycles. LabVIEW software recorded film resistance, intergrip distance, and cycle number.

Acknowledgment. We acknowledge the Science Foundation Ireland funded collaboration (SFI Grant 03/CE3/M406s1) between Trinity College Dublin, University College Cork, and Hewlett-Packard, Dublin Inkjet Manufacturing Operation which allowed this work to take place.

REFERENCES AND NOTES

1. http://www.econstats.com/spot/indium.htm.
2. Chen, Z.; Cotterell, B.; Wang, W. The Fracture of Brittle Thin Films on Compliant Substrates in Flexible Displays. *Eng. Fract. Mech.* **2002**, *69*, 597–603.
3. Leterrier, Y.; Medico, L.; Demarco, F.; Manson, J. A. E.; Betz, U.; Escola, M. F.; Olsson, M. K.; Atamny, F. Mechanical Integrity of Transparent Conductive Oxide Films for Flexible Polymer-Based Displays. *Thin Solid Films* **2004**, *460*, 156–166.
4. Dressel, M.; Gruner, G. *Electrodynamics of Solids: Optical Properties of Electrons in Matter*; Cambridge University Press: Cambridge, 2002.
5. Hu, L.; Hecht, D. S.; Gruner, G. Percolation in Transparent and Conducting Carbon Nanotube Networks. *Nano Lett.* **2004**, *4*, 2513–2517.
6. Aguirre, C. M.; Auvray, S.; Pigeon, S.; Izquierdo, R.; Desjardins, P.; Martel, R. Carbon Nanotube Sheets as Electrodes in Organic Light-Emitting Diodes. *Appl. Phys. Lett.* **2006**, *88*, 183104.
7. Barnes, T. M.; de Lagemaat, J. V.; Levi, D.; Rumbles, G.; Coutts, T. J.; Weeks, C. L.; Britz, D. A.; Levitsky, I.; Peltola, J.; Glatkowski, P. Optical Characterization of Highly Conductive Single-Wall Carbon-Nanotube Transparent Electrodes. *Phys. Rev. B* **2007**, *75*, 235410.
8. Fanchini, G.; Unalan, H. E.; Chhowalla, M. Modification of Transparent and Conducting Single Wall Carbon Nanotube Thin Films *via* Bromine Functionalization. *Appl. Phys. Lett.* **2007**, *90*, 092114.

9. Geng, H. Z.; Kim, K. K.; So, K. P.; Lee, Y. S.; Chang, Y.; Lee, Y. H. Effect of Acid Treatment on Carbon Nanotube-Based Flexible Transparent Conducting Films. *J. Am. Chem. Soc.* **2007**, *129*, 7758–7759 .
10. Geng, H. Z.; Lee, D. S.; Kim, K. K.; Han, G. H.; Park, H. K.; Lee, Y. H. Absorption Spectroscopy of Surfactant-Dispersed Carbon Nanotube Film: Modulation of Electronic Structures. *Chem. Phys. Lett.* **2008**, *455*, 275–278.
11. Gruner, G. Carbon Nanotube Films for Transparent and Plastic Electronics. *J. Mater. Chem.* **2006**, *16*, 3533–3539.
12. Kaempgen, M.; Duesberg, G. S.; Roth, S. Transparent Carbon Nanotube Coatings. *Appl. Surf. Sci.* **2005**, *252*, 425–429.
13. Li, Z. R.; Kandel, H. R.; Dervishi, E.; Saini, V.; Xu, Y.; Biris, A. R.; Lupu, D.; Salamo, G. J.; Biris, A. S. Comparative Study on Different Carbon Nanotube Materials in Terms of Transparent Conductive Coatings. *Langmuir* **2008**, *24*, 2655–2662.
14. Parekh, B. B.; Fanchini, G.; Eda, G.; Chhowalla, M. Improved Conductivity of Transparent Single-Wall Carbon Nanotube Thin Films *via* Stable Postdeposition Functionalization. *Appl. Phys. Lett.* **2007**, *90*, 121913.
15. Pasquier, A. D.; Unalan, H. E.; Kanwal, A.; Miller, S.; Chhowalla, M. Conducting and Transparent Single-Wall Carbon Nanotube Electrodes for Polymer-Fullerene Solar Cells. *Appl. Phys. Lett.* **2005**, *87*, 203511.
16. Wu, Z. C.; Chen, Z. H.; Du, X.; Logan, J. M.; Sippel, J.; Nikolou, M.; Kamaras, K.; Reynolds, J. R.; Tanner, D. B.; Hebard, A. F.; Rinzler, A. G. Transparent, Conductive Carbon Nanotube Films. *Science* **2004**, *305*, 1273–1276.
17. Yim, J. H.; Kim, Y. S.; Koh, K. H.; Lee, S. Fabrication of Transparent Single Wall Carbon Nanotube Films with Low Sheet Resistance. *J. Vac. Sci. Technol., B* **2008**, *26*, 851–855.
18. Zhang, D. H.; Ryu, K.; Liu, X. L.; Polikarpov, E.; Ly, J.; Tompson, M. E.; Zhou, C. W. Transparent, Conductive, and Flexible Carbon Nanotube Films and their Application in Organic Light-Emitting Diodes. *Nano Lett.* **2006**, *6*, 1880–1886.
19. Lyons, P. E.; De, S.; Blighe, F.; Nicolosi, V.; Pereira, L. P. C.; Ferreira, M. S.; Coleman, J. N. the Relationship between Network Morphology and Conductivity in Nanotube Films. *J. Appl. Phys.* **2008**, *104*, 044302.
20. Bauhofer, W.; Kovacs, J. Z. A Review and Analysis of Electrical Percolation in Carbon Nanotube Polymer Composites. *Compos. Sci. Technol.* **2008**, in press.
21. Blighe, F.; Hernandez, Y.; Blau, W. J.; Coleman, J. N. Observation of Percolation-like Scaling—Far from the Percolation Threshold—In High Volume Fraction, High Conductivity Polymer−Nanotube Composite Films. *Adv. Mater.* **2007**, *19*, 4443–4447.
22. Guo, H.; Sreekumar, T. V.; Liu, T.; Minus, M.; Kumar, S. Structure and Properties of Polyacrylonitrile/Single Wall Carbon Nanotube Composite Films. *Polymer* **2005**, *46*, 3001–3005.
23. Ham, H. T.; Choi, Y. S.; Chee, M. G.; Cha, M. H.; Chung, I. J. PEDOT-PSS/Singlewall Carbon Nanotubes Composites. *Polym. Eng. Sci.* **2008**, *48*, 1–10.
24. Moon, J. S.; Park, J. H.; Lee, T. Y.; Kim, Y. W.; Yoo, J. B.; Park, C. Y.; Kim, J. M.; Jin, K. W. Transparent Conductive Film Based on Carbon Nanotubes and PEDOT Composites. *Diamond Relat. Mater.* **2005**, *14*, 1882–1887.
25. Mustonen, T.; Kordas, K.; Saukko, S.; Toth, G.; Penttilla, J. S.; Helisto, P.; Seppa, H.; Jantunen, H. Inkjet Printing of Transparent and Conductive Patterns of Single-Walled Carbon Nanotubes and PEDOT-PSS Composites. *Phys. Status Solidi B* **2007**, *244*, 4336–4340.
26. Wang, W.; Fernando, K. A. S.; Lin, Y.; Meziani, M. J.; Veca, L. M.; Cao, L.; Zhang, P.; Kimani, M. M.; Sun, Y. P. Metallic Single-Walled Carbon Nanotubes for Conductive Nanocomposites. *J. Am. Chem. Soc.* **2008**, *130*, 1415–1419.
27. Wang, G. F.; Tao, X. M.; Wang, R. X. Flexible Organic Light-Emitting Diodes with a Polymeric Nanocomposite Anode. *Nanotechnology* **2008**, *19*, 145201.
28. Crispin, X.; Jakobsson, F. L. E.; Crispin, A.; Grim, P. C. M.; Andersson, P.; Volodin, A.; van Haesendonck, C.; Van der Auweraer, M.; Salaneck, W. R.; Berggren, M. The Origin of the High Conductivity of Poly(3,4-ethylenedioxythiophene)-poly(styrenesulfonate) (PEDOT-PSS) Plastic Electrodes. *Chem. Mater.* **2006**, *18*, 4354–4360.
29. Ruzicka, B.; Degiorgi, L.; Gaal, R.; Thien-Nga, L.; Bacsa, R.; Salvetat, J. P.; Forro, L. Optical and DC Conductivity Study of Potassium-Doped Single-Walled Carbon Nanotube Films. *Phys. Rev. B* **2000**, R2468–R2471.
30. Kilbride, B. E.; Coleman, J. N.; Fraysse, J.; Fournet, P.; Cadek, M.; Drury, A.; Hutzler, S.; Roth, S.; Blau, W. J. Experimental Observation of Scaling Laws for Alternating Current and Direct Current Conductivity in Polymer−Carbon Nanotube Composite Thin Films. *J. Appl. Phys.* **2002**, *92*, 4024–4030.
31. Dikin, D. A.; Stankovich, S.; Zimney, E. J.; Piner, R. D.; Dommett, G. H. B.; Evmenenko, G.; Nguyen, S. T.; Ruoff, R. S. Preparation and Characterization of Graphene Oxide Paper. *Nature* **2007**, *448*, 457–460.